Materials Letters 99 (2013) 111–114

Contents lists available at SciVerse ScienceDirect

Materials Letters

journal homepage: www.elsevier.com/locate/matlet

Synthesis, optical and magnetic properties of α-Fe_2O_3 nanoparticles with various shapes

Xin Zhang [a], Yongan Niu [b], Yao Li [b], Xuemei Hou [a], Yibo Wang [a], Rui Bai [a], Jiupeng Zhao [a,*]

[a] School of Chemical Engineering and Technology, Harbin Institute of Technology, Harbin 150001, PR China
[b] Center for Composite Materials, Harbin Institute of Technology, Harbin 150001, PR China

ARTICLE INFO

Article history:
Received 27 December 2012
Accepted 17 February 2013
Available online 26 February 2013

Keywords:
α-Fe_2O_3
Nanoparticles
Hydrothermal synthesis
Magnetic materials
Shape-dependent effect

ABSTRACT

The various shapes of α-Fe_2O_3 nanoparticles were successfully prepared via hydrothermal and solvothermal synthesis. The morphologies and crystalline structures were controlled by different catalysts. Compared with others, the spindle α-Fe_2O_3 nanoparticle exhibited excellent optical and magnetic properties. Its optical band gap was at 2.05 eV, calculated by the Tauc plot method. The magnetic hysteresis loops demonstrated that remanent magnetization (M_r) was of 0.0951 emu/g and coercivity (H_c) was of 1645 Oe. Furthermore, the results revealed that the structure of the α-Fe_2O_3 had a remarkable shape-dependent effect on the optical and magnetic properties.

1. Introduction

Synthesis of inorganic nanoparticles with homogeneous size and shape have attracted extensive attention due to the innovative physical and chemical properties [1]. Recently, the controllable synthesis of α-Fe_2O_3 nanoparticles has become a new focus of material studies. They have a wide range of applications in catalytic agents [2], magnetic recording materials [3], gas sensors [4], lithium-ion batteries [5] and drug delivery [6]. Various shapes of α-Fe_2O_3 nanoparticles, such as nanowires, plates, cubes, rods and tubes, have been prepared by hydrothermal and solvothermal routes [7,8]. However, research on α-Fe_2O_3 nanoparticle has been previously centered on its synthesis method and crystal growth mechanism. The relationship between the structure and physical properties was rarely reported [9].

In this study, we successfully synthesized four shapes of monodispersed α-Fe_2O_3 nanoparticles by the simple hydrothermal and solvothermal routes. This work was aimed to investigate the relationship between the structure factors, i.e., free surface, grain boundaries, preferred orientation, and the optical and magnetic properties. The majors were growth orientation and shapes of the α-Fe_2O_3 nanoparticles.

2. Experimental section

α-Fe_2O_3 nanoparticles were prepared by hydrothermal and solvothermal routes. 0.03 mmol of catalysts (i.e., NaH_2PO_4, dilute hydrochloric acid or L-lysine) was dissolved in 30 mL of 0.02 M $FeCl_3$ aqueous solution. The solution was put into a 100 mL Teflon-lined autoclave. The autoclave was sealed and maintained at 120 °C for 24 h, and then cooled to room temperature. In addition, 0.01 mmol of polyvinylpyrrolidone (PVP, M_w=360,000) was dissolved in 30 mL of 0.02 M $FeCl_3$ in DMF solution. It was placed at a temperature of at 200 °C for 24 h in an oven. The as-prepared precipitates were washed with distilled water and absolute ethanol several times, and finally dried at 60 °C for 24 h in air.

The structures and morphologies of the as-prepared samples were characterized by powder X-ray diffraction (XRD, D/max-rB 12KW), scanning electron microscopy (SEM, QUANTA 200F), and transmission electron microscopy (TEM, Tecnai G^2 F30). The optical properties were recorded by a UV–vis absorption spectrometer (UV-2550PC) at the wavelength ranging from 200 to 800 nm. Magnetic properties at room temperature were measured by a vibrating sample magnetometer (VSM, Lake Shore7407) in a maximum field of 15 kOe.

3. Results and discussion

Fig. 1 shows the XRD patterns of the as-prepared α-Fe_2O_3 samples. All the diffraction peaks were indexed to the rhombohedral structure of hematite α-Fe_2O_3, which were in good agreement with JCPDS no. 33-0664. The sharp diffraction peaks indicated good crystallinity of the samples. The XRD patterns did not show any traces of other phases of Fe_2O_3, thus they performance the high purity for as-obtained α-Fe_2O_3 samples. The (110) peak of the quasi-cubic sample was stronger than

* Corresponding author. Tel./fax: +86 451 86403767.
E-mail address: jiupengzhao@126.com (J. Zhao).

0167-577X/$ - see front matter © 2013 Elsevier B.V. All rights reserved.
http://dx.doi.org/10.1016/j.matlet.2013.02.070

others, which demonstrated that the sample exists in the preferred orientation in a variety of directions.

Fig. 2(a, d, g and j) displayed typical HRTEM images of four samples. Their average diameters ranged from 90 to 110 nm at the minor axis. Because of influence of $H_2PO_4^-$ on the growth behavior, the [001] direction grew faster than others [10], the spindle sample had a preferred orientation in direction of the [001] axis, as shown in Fig. 2(b). According to Fig. 2(c), the spindle sample attached and had identical lattice fringes with *d* spacings of 0.230 nm and 0.369 nm, which was in agreement with the (006) and (012) facets, respectively. Moreover, the lattice fringe spacings in HRTEM images (Fig. 2f and i) exhibited that the ellipsoid and like-spherical samples had lower preferential orientation than the spindle sample, which also clearly was demonstrated by SAED data in Fig. 2(e and h). As shown in Fig. 2(k and l), the lattice plane spacings of the quasi-cubic sample were 0.370 nm and 0.370 nm, which corresponded to the {012} planes of a rhombohedral [11]. It indicated that the quasi-cubic sample had the lowest preferred orientation among four samples. Furthermore, compared with the free surface of the four samples, the spindle sample was larger than others. With the crystalline growth in the single axis, defects like grain boundaries in the spindle sample obviously appeared to be attributed to preferred orientation. The optical and magnetic properties were also enhanced by changes of the free surface and grain boundaries [12].

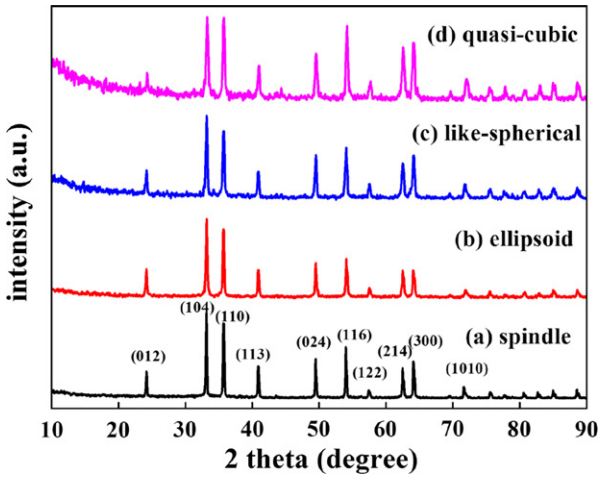

Fig. 1. XRD patterns of the α-Fe_2O_3 samples by hydrothermal and solvothermal routes with (a) spindle, (b) ellipsoid, (c) like-spherical, and (d) quasi-cubic morphologies.

UV–vis absorption spectra of all four samples are showed in Fig. 3(a). There were two types of absorption bands observed for different samples. The first peak at 270 nm was assigned to metal to ligand charge transfer spectra. For (b) spindle and (c) ellipsoid samples, the second peaks between 455 nm and 538 nm were more prominent than others, which is considered to be the result of pair excitation processes, ligand field transitions and charge-transfer band tails [13]. As an n-type semiconductor of indirect band gap, the optical band gap energy (E_g) could be calculated by using the following equation, and the Tauc plot method from this region of the UV–vis spectra [14].

$$(\alpha h\upsilon)^n = B(h\upsilon - E_g) \quad (1)$$

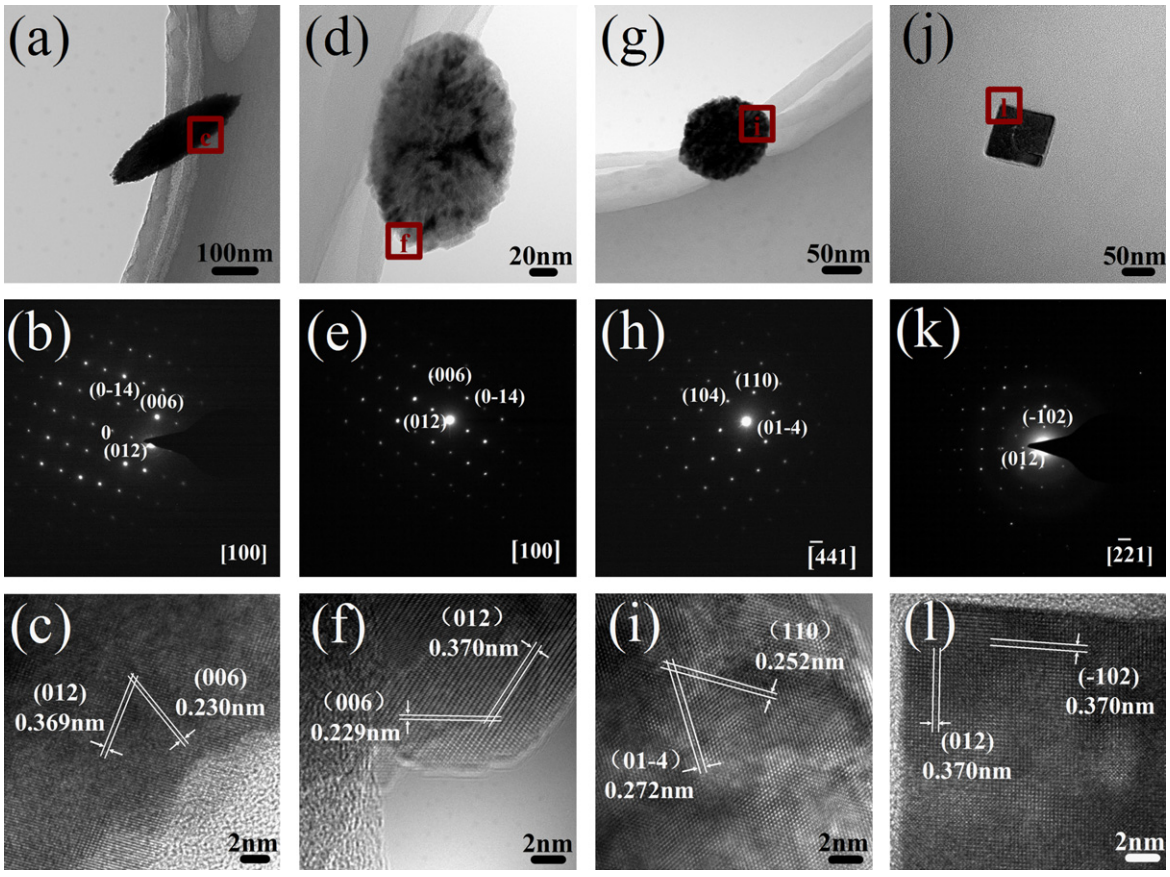

Fig. 2. HRTEM images of the as prepared α-Fe_2O_3 of (a, c) spindle particle, (d, f) ellipsoid particle, (g, i) like spherical particle, and (j, l) quasi-cubic particle; (b, e, h, k) are their SEAD patterns, respectively.

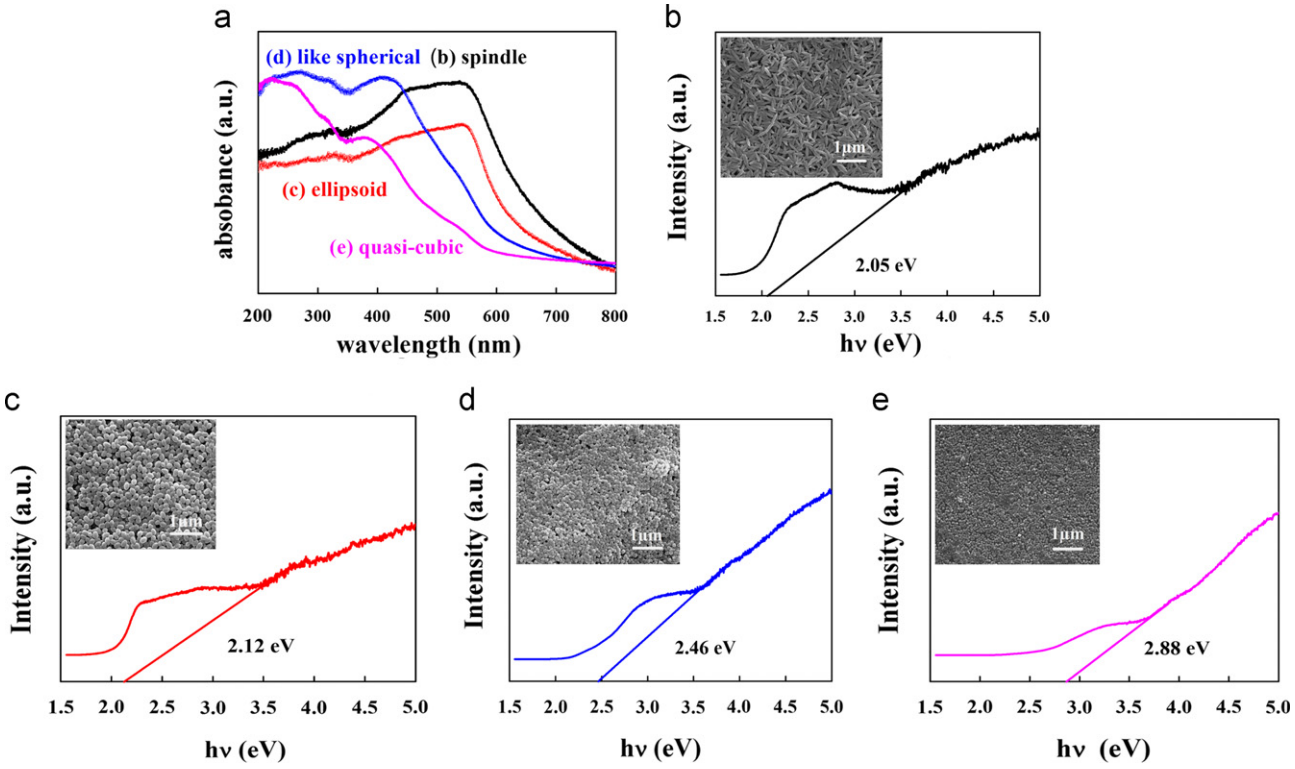

Fig. 3. (a) Shape-dependent UV–vis absorption spectra of as-prepared samples. The optical band gaps of as-prepared (b) spindle, (c) ellipsoid, (d) like spherical and (e) quasi-cubic samples estimated by the Tauc plot method. The inserts of (b–e) are SEM images of corresponding samples, respectively.

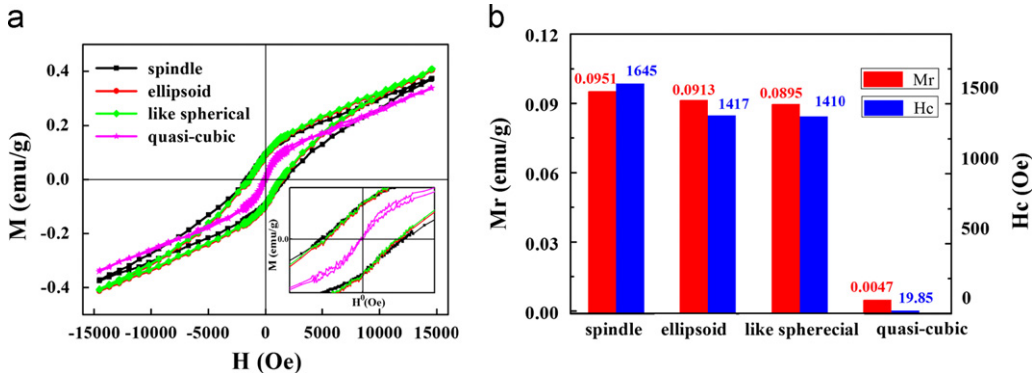

Fig. 4. (a) Magnetization curves measured at room temperature of as-prepared samples. (b) Values of remanent magnetization (M_r) and coercivity (H_c) of as-prepared samples.

where α is the absorption coefficient, $h\upsilon$ is the photo energy, and B is the material-dependent constant.

The independent spectra of four samples are shown in Fig. 3(b–e) and the inserts were SEM images of the corresponded samples. The obtained E_g values were 2.05 eV for spindle, 2.12 eV for ellipsoid, 2.46 eV for like spherical and 2.88 eV for quasi-cubic samples, respectively. The results showed that there were obvious blue shifts compared with the bulk α-Fe_2O_3 (2.1 eV), which could be due to the quantum size effect [15]. However, the E_g of spindle sample was lower than that of the bulk α-Fe_2O_3. Due to the preferred orientation in single axis, the shape-dependent effect would become a main impact factor of optical properties.

α-Fe_2O_3 nanoparticles often display the unusual magnetic behavior [16]. Due to the free surface and grain boundaries, the magnetic properties improved [17]. Fig. 4(a) shows the magnetic hysteresis loops of the as-prepared samples at room temperature. The results indicated that they have weak ferromagnetic behavior. The saturation magnetization was not observed in the magnetization field. Fig. 4(b) demonstrates the values of remanent magnetization (M_r) and coercivity (H_c). For spindle, ellipsoid and like spherical samples, the values were almost approximate. However, for the quasi-cubic sample, it exhibited an extremely small magnetization and weak hysteresis loop behavior, because it had the lowest preferred orientation among the all samples in this study. Moreover, for the spindle sample, it displayed the highest magnetic properties with M_r of 0.0951 emu/g and H_c of 1645 Oe. It must be owing to the influence of preferred orientation in single axis [18]. Therefore, the magnetization also has a shape-depended behavior for α-Fe_2O_3 samples.

4. Conclusions

In summary, α-Fe_2O_3 nanoparticles with various shapes, i.e., spindle, ellipsoid, like spherical and quasi-cubic, have been successfully prepared via the hydrothermal and solvothermal routes in

presence of different catalysts. All the samples were well-defined α-Fe_2O_3 nanocrystals as seen by XRD and TEM. In particular, the spindle sample exhibited outstanding optical and magnetic properties due to the shape-dependent effect. These results not only enrich the magnetic theory of α-Fe_2O_3 nanoparticles, but also provide a new strategy to design the magnetic materials, which would be useful for lithium-ion batteries and gas sensors.

Acknowledgments

We thank National Natural Science Foundation of China (Nos. 51010005, 91216123, and 51174063), the program for New Century Excellent Talents in University (NCET-08–0168), Natural Science Funds for Distinguished Young Scholar of Heilongjiang Province. The Project of International Cooperation was supported by Ministry of Science and Technology of China (2013DFR10630).

References

[1] Almeida TP, Fay M, Zhu YQ, Brown PDJ. Phys Chem C 2009;113:18689–98.
[2] Jiao SH, Chen Y, Man X, Zhang YW, Wang D, Pang GS, et al. Mater Lett 2010;64:1704–6.
[3] Zeng SY, Tang KB, Li TWJ. Colloid Interface Sci 2007;312:513–52.
[4] Wu CZ, Yin P, Zhu X, OuYang CZ, Xie YJ. Phys Chem B 2006;110:17806–12.
[5] Sun B, Horvat J, Kim HS, Kim WS, Ahn JH, Wang GXJ. Phys Chem C 2010;114:18753–61.
[6] Chen Y, Chen HR, Zeng DP, Tian YB, Chen F, Feng JW, et al. ACS Nano 2010;4:6001–13.
[7] Gupta RK, Ghosh K, Dong L, Kahol PK. Mater Lett 2010;64:2132–4.
[8] Jia CJ, Sun LD, Yan ZG, You LP, Luo F, Han XD, et al. Angew Chem Int Ed 2005;44:4328–33.
[9] Lian JB, Duan XC, Ma JM, Peng P, Kim T, Zheng WJ. ACS Nano 2009;3:3749–61.
[10] Lv BL, Xu Y, Wu D, Sun YH. Cryst Eng Comm 2011;13:7293–8.
[11] Yin WY, Chen X, Cao MH, Hu CW, Wei BQJ. Phys Chem C 2009;113:15897–903.
[12] Frentrup M, Ploch S, Pristovsek M, Kneissl M. Phys Status Solidi B 2011;248:583–7.
[13] Zhang JT, Liu JF, Peng Q, Wang X, Li YD. Chem Mater 2006;18:867–71.
[14] He YP, Miao YM, Li CR, Wang SQ, Cao L, Xie SS, et al. Phys Rev B 2005;71:125411.
[15] Mitra S, Das S, Manda K, Chaudhuri S. Nanotechnology 2007;18:275608.
[16] Ni H, Ni YH, Zhou YY, Hong JM. Mater Lett 2012;73:206–8.
[17] Straumal BB, Mazilkin AA, Protasova SG, Myatiev AA, Straumal PB, Goering E, et al. Thin Solid Films 2011;520:1192–4.
[18] Ngo AT, Pileni MP. Colloids Surf A Physicochem Eng Aspects 2003;228:107–17.